

EUROPEAN LABORATORY FOR PARTICLE PHYSICS (CERN)

CERN-EP 99-166
28 October 1999

A four-gap glass-RPC time-of-flight array with 90 ps time resolution

A. Akindinov¹, P. Fonte^{2,3,*}, F. Formenti², V. Golovine¹, W. Klempt², A. Kluge²,
A. Martemiyarov¹, P. Martinengo², J. Pinhão³, A. Smiritski¹,
M. Spegel^{2,‡}, P. Szymanski^{2,4}, J. Zalipska^{2,5}

¹*ITEP, Moscow, Russian Federation*, ²*CERN, Geneva, Switzerland*, ³*LIP, Coimbra, Portugal*,

⁴*Inst. for Nuclear Studies, Warsaw, Poland*, ⁵*Univ. of Warsaw, Warsaw, Poland*

* *On leave of absence from ISEC, Coimbra, Portugal*

‡ *corresponding author, Marko.Spegel@cern.ch*

Abstract

In this work we describe the performance of a prototype developed in the context of the ALICE time-of-flight R&D system. The detector module consists of a 32-channel array of 3 x 3 cm² glass-RPC cells, each of which has four accurately spaced gaps of 0.3 mm thickness arranged as a pair of double-gap resistive plate chambers. Operated with a non-flammable gas mixture at atmospheric pressure, the system achieved a time resolution of 90 ps at 98% efficiency with good uniformity and moderate crosstalk. This result shows the feasibility of large-area, high resolution time-of-flight systems based on RPCs at affordable cost.

(Submitted to IEEE transactions on Nuclear Science)

1 Introduction

In the framework of R&D for the ALICE time-of-flight system [1] and following earlier work [2] we designed, constructed and tested an array of 32 cells of multi-gap resistive plate chambers (RPCs) as a basic building block for large ($> 1 \text{ m}^2$) TOF modules. Among its main properties, one may stress the small current pulses in case of discharge, moderate cross-talk between channels, the high detection efficiency, and in particular, very good time resolution.

2 Description of detector

2.1 Glass-RPC detector cell

The detector cells are constituted by a pair of identical double-gap chambers (Figure 1), each made of aluminium anode and cathode and a central resistive glass plate at floating potential. The cathodes are connected to a negative high voltage and the anodes, kept at ground potential through a $10 \text{ M}\Omega$ resistor, are connected together and feed the amplifier. The glass plate, made from standard Nr. 10 welding glass [3], has a resistivity $\rho \approx 2 \times 10^{12} \Omega \text{ cm}$. The size of all plates is $32 \times 32 \text{ mm}^2$, with a thickness of 2 mm for the aluminium plates and 3 mm for the glass plates. The rounded edges of the aluminium plates leave an active area of $30 \times 30 \text{ mm}^2$.

The different elements are assembled in a plastic box that provides electrical insulation and mechanical rigidity. This box has holes for wires connected to the metallic electrodes, for gas circulation and for insertion of spacers that define the gaps. These spacers are short pieces of optical glass fiber ($\varnothing 0.3 \text{ mm}$), that are inserted in the four corners of the chamber in each gap. Further construction details can be found in reference [4].

2.2 32-channel array

The detector cells are arranged in an array of four times eight squares, following a chessboard-like pattern in two layers (Figure 2). The edges of the active areas in the two layers are aligned, providing a geometrical coverage of 97% for normal incidence angle. Mechanical support for the cells is provided by plastic spacers glued onto the detector PCB, which carries the high voltage circuitry, signal feed-throughs to the readout electronics, and provides gas tightness on one surface of the gas volume.

The schematics of the high voltage distribution (Figure 3) features multi-level high-voltage filtering to assure stable operation of the first prototype. The physical layout is carefully optimized to suppress crosstalk between neighboring channels across the electrical connections. In particular the signal ground is separated from the HV ground for optimum pick-up noise and crosstalk rejection, rendering adjacent cells almost electrically independent.

Figure 4 shows the physical layout of one high voltage distribution unit of $6 \times 12 \text{ cm}^2$ serving eight detector cells. All metallic parts on both sides of the PCB which are on HV potential are concentrated in the center of the unit and covered by protective glue [5] to avoid surface currents and discharges. The surrounding ground loop encloses a surface of $\sim 50 \text{ cm}^2$ only, hence it is rather insensitive to external high frequency noise. The four 8-cell units of the PCB for the 32-cell module are interconnected by HV and ground jumpers to be supplied by one HV line.

For our tests, the detector PCB carrying the array of 32 cells was mounted in a metallic box that closed the gas volume, carried gas connections and allowed the module to be fixed to a

moving table. All six faces of the box were covered by a thin PCB with a copper layer connected to HV ground for electrical shielding, leaving only small holes for the connectors to the readout electronics.

2.3 Readout electronics

The design of the readout electronics was guided by the requirement to resemble as closely as possible the foreseen implementation scheme for the ALICE time-of-flight system [6]. A prototype signal pickup card contained shaping amplifiers, discriminators and edge detecting circuitry for eight channels (Figure 5). Four cards were attached orthogonally to the detector PCB via connectors for chamber signals and, optionally, the high voltage ground. The connectors for low voltage, test signal input, and analog and digital outputs were placed at the opposite edge of the card.

Custom amplifiers with a rise time of less than 1.8 ns which were built from discrete components were plugged onto the signal pickup card. The width of the output signal is related to the input charge and lies in a range of 15 to 50 ns, allowing the measurement of the input signal amplitude as time-over-threshold.

The fixed threshold discriminator scheme with a hysteresis of 14 mV is based on a commercial ECL comparator (AD96685BR). Circuitry using components from the 10EL family detects leading and trailing edges corresponding to time-of-flight and input signal amplitude respectively.

Furthermore, the card layout features:

- physical location of amplifiers and ECL components close to the detector cells for minimum signal path lengths;
- on-board low voltage regulation for all components in groups of four channels;
- jumper-selectable test signal distribution;
- buffered analog output for an optional signal amplitude measurement via an ADC

With 20 m of 100 Ω twisted pair flat cable (3M 2100) between the prototype cards and TDC electronics, an electronics time resolution of the leading edge signal of 45 ± 9 ps (Figure 6) and a total system noise level below 1 fC could be achieved. Significantly better performance can be expected from a version of the signal pickup card containing amplifier-shapers, discriminators and TDCs for 16 readout channels, where all analog and discrimination circuitry would be integrated on an four channel ASIC chip.

3 Experimental setup

The detector tests were carried out at the CERN-PS using a secondary beam (T10) of 7 GeV/c negative pions in 0.25 s long spills. The defocussed beam illuminated a detector cell almost uniformly with an intensity of ~ 600 Hz/cm².

The glass-RPC array was operated in a continuously flowing non-flammable gas mixture of 85% C₂H₂F₄, 10% SF₆, and 5% isobutane at atmospheric pressure [7].

Three pairs of multi-wire proportional chambers with cathode strip readout allowed tracking with sub-millimeter precision in both coordinates orthogonal to the beam. A pair of scintillator counters, each equipped with two photomultipliers placed at both ends of the scintillator slab, provided a time reference of ~ 50 ps resolution.

All timing channels were measured using LeCroy 2228A TDCs with 50 ps bin width (except trailing edge signals with 250 ps), and amplitude channels with LeCroy 2249A ADCs

with a gate width of 150 ns.

4 Data analysis

Events passing the following criteria were selected for further analysis (leaving typically 20% of the 10000 events per run):

- A particle position within $\pm 2 \sigma$ around the beam center in both coordinates.
- One charge cluster in each of the six tracking chamber planes (to remove events with more than one beam particle).
- A time difference between the two scintillator counters within $\pm 2 \sigma$ around the mean value of the distribution for all events.
- An average charge sum of both photomultipliers of each scintillator counter within $\pm 2 \sigma$ around the mean value.

Since the measured time is correlated to the analog signal amplitude, we apply the following time-amplitude correction procedure to the data:

For each event, a reference time measured by the scintillator counters was subtracted. This time difference is shown as a function of signal amplitude in Figure 7. The width of the band on this figure is given by the time resolution of a detector convoluted with the electronics resolution and the time reference resolution. The time-amplitude dependence was parametrized by linear fits for ten slices in amplitude containing equal numbers of events. For each event a corrected time was obtained as the difference between the measured time and the value of the correction function corresponding to the pulse amplitude for this particular event. Therefore the mean value of corrected times is zero.

A Gaussian function was fitted to a distribution of a corrected time in a range of $\pm 1.5 \sigma$ around the mean value (Figure 8). To obtain the time resolution of the tested detector channel, the reference time resolution of 50 ps was subtracted quadratically from the fit result.

The results presented in this paper were obtained with time-amplitude correction applied separately for each data set. However, a correction of several subsequent runs at the same run conditions with the same correction function did not alter the obtained resolution significantly.

5 Results

The properties of signals from a glass-RPC cell and their dependence on a discriminator threshold, detector high voltage and a beam intensity has been extensively studied in single cell tests [4] and for some cells of the array. Results described below were obtained with optimal values of high voltage (5800 V) and discriminator threshold (20 fC).

5.1 Single cells

Figure 9 shows the typical shape of a proportional signal from a glass-RPC cell seen directly on the oscilloscope with 50 Ω termination. The fast charge is about 0.5 pC. Pulse height spectra at different operating voltages are presented in Figure 10. At the standard operating voltage of 5800V, the fast signal has an average charge of ~ 1 pC, and discharges occur with small ($< 1\%$) probability in the form of streamer pulses of limited charge (~ 20 pC) [4].

In the present design, the detector cells exhibit a certain level of dark counts (Figure 11). These originate mainly from the region of the glass fibre spacers, their pulse height was found to be significantly lower than proportional signals from particles, and the dark count rate is an

order of magnitude lower than the particle rate per cell expected for the ALICE environment.

The dependence of the detector performance on the operating voltage can be seen in Figure 12. Within the spread of different measurements at the same conditions (~ 10 ps), the resolution curve is flat from 5200 V up to 6600 V. At lower voltages the resolution suffers from decreasing pulse height of the proportional signals, at higher values the increasing probability for streamer pulses slightly deteriorates the detector performance. The intrinsic detector efficiency stays better than 95% above 5200V.

The discrimination threshold can be varied by more than an order of magnitude without significant impact on the timing performance (Figure 13), which leaves a wide margin for performance optimization: a higher threshold will further decrease the crosstalk probability (see below), a lower threshold can be translated into a smaller electronics gain requirement.

Measurements of the detector performance at different particle rates showed stable performance up to ~ 1 kHz/cm² (Figure 14), which is far above the expected rate of 200 Hz/cm² in the ALICE experiment. However, the short spill duration of 0.25 s does probably not correctly reflect the situation in the experiment due to dynamic effects. Tests with a radioactive source inducing a DC current of ~ 4 nA at an additional count rate of 150 Hz/cm² did not induce any visible deterioration of the cell performance.

5.2 32-cell array

The distribution of measured time resolutions for 31 detector channels¹ has a mean value of 89 ps with an RMS error of 9 ps (Figure 15). The use of optimized readout electronics with 20 ps resolution on one cell in the array improved the time resolution from 87 ps to 75 ps in agreement with single cell tests. Measurements of selected cells with inclined beam (20° and 40°) or lower beam energy (1 GeV/c) yielded similar timing performance.

From first tests using the pulse width instead of the ADC value for the amplitude correction of one cell we obtained 89 ps (time-width-correction) instead of 81 ps (time-amplitude-correction). More appropriate pulse shaping in future amplifiers will assure equal performance of both amplitude measurements. The mean cell efficiency is 98% (Figure 16) with an excellent uniformity over the sample (1% RMS error).

We found the analog crosstalk between adjacent channels to be almost entirely due to capacitive coupling between the cells, inducing in these channels analog signals of inverse polarity and an amplitude of $\sim 1\%$ of that in the cell hit by a particle. In our analysis, crosstalk from the detector cell hit by a beam particle to other channels was quantified as the probability of getting a signal above the discriminator threshold in a cell not hit by a beam particle. We calculate an average over all channels in the module (crosstalk) and over channels adjacent to a hit cell (crosstalk to neighbors).

The mean crosstalk was found to be 0.2% (Figure 17), and the mean crosstalk to neighbors was 0.6% (Figure 18) with a large relative spread (65%). The latter is most probably caused by variations in the cell spacing due to low cell positioning precision in the prototype module.

6 Conclusions

We designed, built and tested a 32-channel array of 3 x 3 cm² glass-RPCs [4]. Operated in a non-flammable gas mixture at atmospheric pressure, such cells showed stable performance below 90 ps throughout an operating voltage range of more than 1 kV, for counting rates up to

1. One readout channel was modified for special studies.

several hundred Hz/cm², and for discrimination thresholds varying over more than an order of magnitude. The use of thinner and less resistive glass plates should further increase the rate capabilities of the detector. The optimum discrimination threshold was 20 fC, well above the 1 fC electronics noise level and far below the mean pulse charges (~ 1 pC), providing a large safety margin against system-generated noise or crosstalk from adjacent cells.

The 32-cell array performed very well with mean time resolution 89 ps, mean efficiency 98%, and mean crosstalk 0.2%. There is ample room for further improvement — for example, optimized readout electronics which was tested on one of the module channels improved time resolution from 87 ps to 75 ps. A similar, slightly modified glass-RPC has shown resolutions as low as 50 ps [4].

The performance of the glass-RPCs seems to be fairly insensitive to changes in the operating conditions, i.e., temperature, pressure, high voltage, discrimination threshold, particle incident angle, or particle rate.

The main features of this detector — simple and mechanically stable construction, very good and uniform time resolution and detection efficiency, large operating plateau, high discrimination threshold, and small intrinsic crosstalk — prove the suitability of this approach for the construction of large-area time-of-flight arrays.

Acknowledgments

We would like to thank the CERN PS group for very stable operation of the accelerator during test periods. The help of members of CERN EP/TA2 and EP/AIT groups in the preparation and running of the test beam setup is kindly acknowledged. The construction of the detector cells at LIP-Coimbra was financed by the portuguese ICCTI/FCT, via contract CERN/FAE/1197/98.

References

- [1] ALICE Collaboration, *Technical Proposal*, LHCC-P3 and CERN-LHCC-95-71
- [2] E. Cerron-Zeballos et al., *A new type of resistive plate chamber: the multigap RPC*, NIM A 374 (1996) 132.
P. Fonte, A. Smirnitski and M.C.S. Williams, *A new high-resolution TOF technology*, CERN-EP-99-68. Submitted to Nuclear Instrumentation and Methods A.
- [3] SCHOTT ATHERMAL(r) 10 A1 DIN
- [4] P. Fonte et al., *High Resolution RPCs for Large TOF Systems*, CERN-EP-99-115. Submitted to Nuclear Instrumentation and Methods A.
- [5] CIBA Araldite, resine AW 106 and hardener HV 953 U.
- [6] A. Kluge, *Study of the Alice Time of Flight Readout System — AFRO*, Proceedings of the fifth workshop for electronics for LHC experiments, Snowmass, USA, September 1999.
A. Kluge, *ALICE Time of Flight Readout — AFRO: Study of Requirements and Architecture*, ALICE-INT-99-40
- [7] P. Camarri et al., *Streamer suppression with SF₆ in RPCs operated in avalanche mode*, NIM A414 (1998) 317.

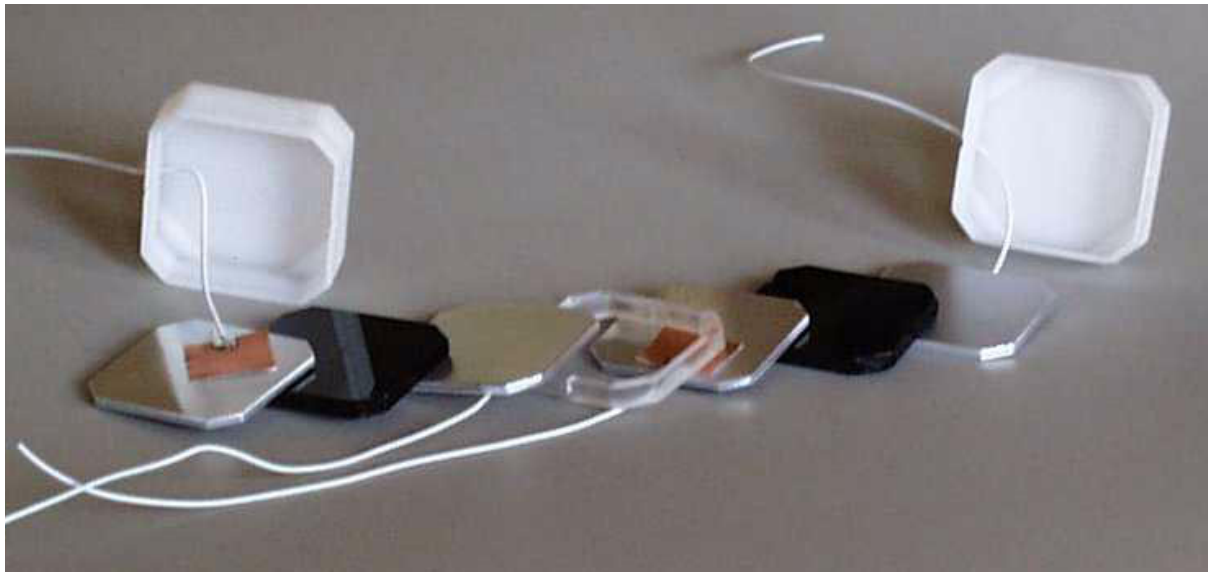


Figure 1: Relative position of the various elements that compose one cell. The spacers (glass fibers) are the only elements not shown in the picture.

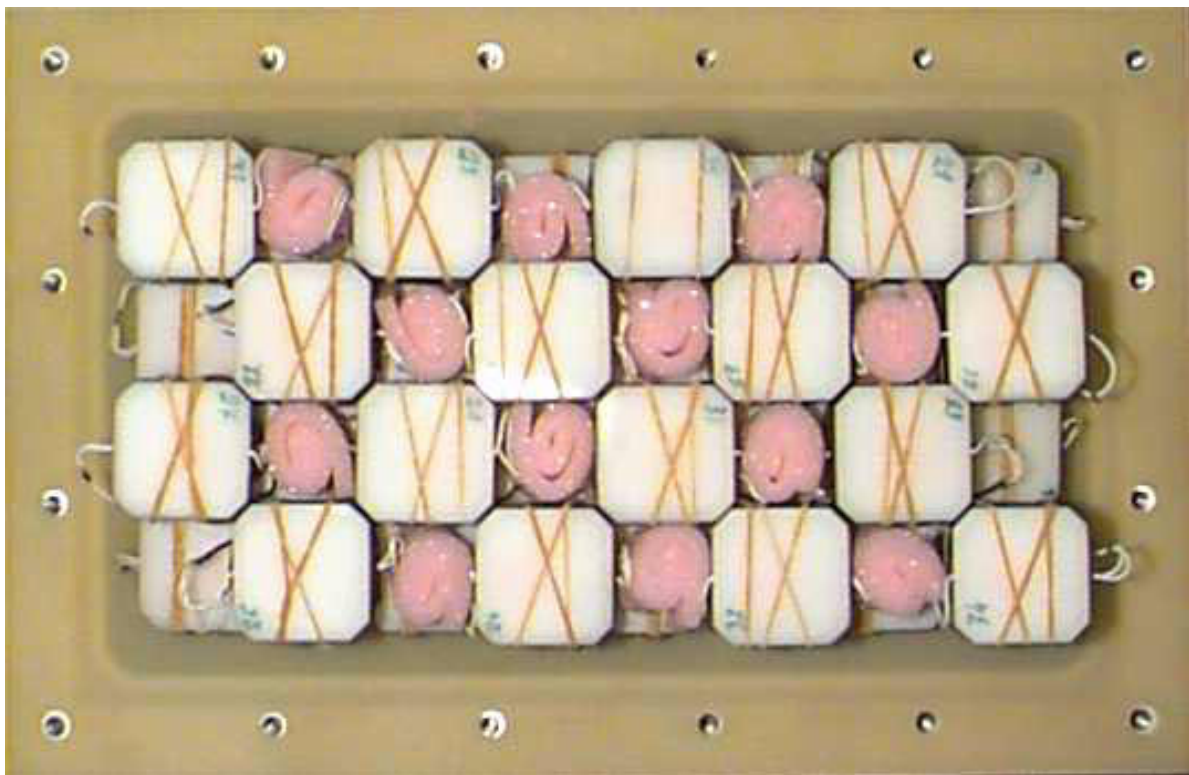


Figure 2: Arrangement of the 32 detector cells in two layers following a chessboard-like pattern.

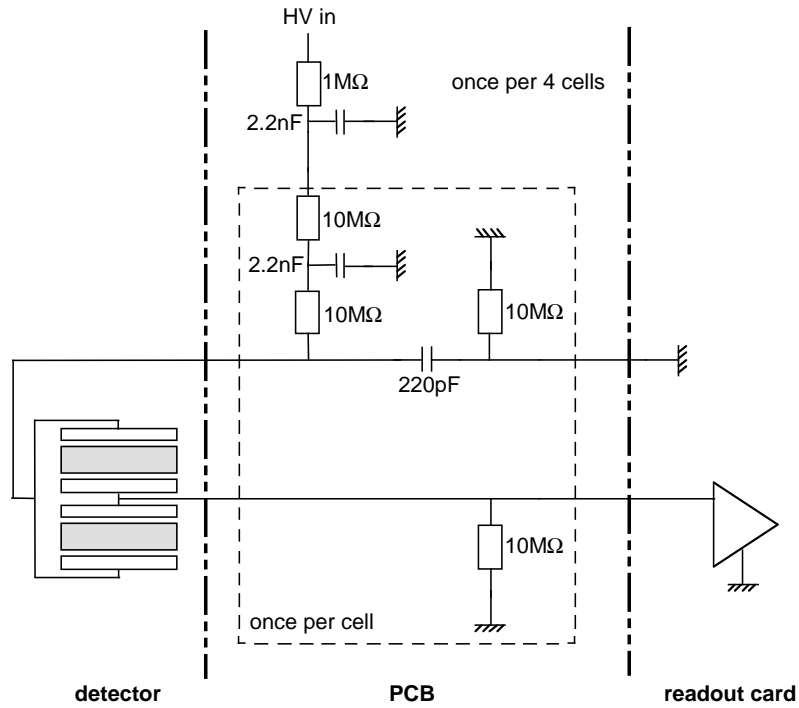


Figure 3: Schematics of the electrical connectivity of the array. The amount of HV filters might be reduced in future versions.

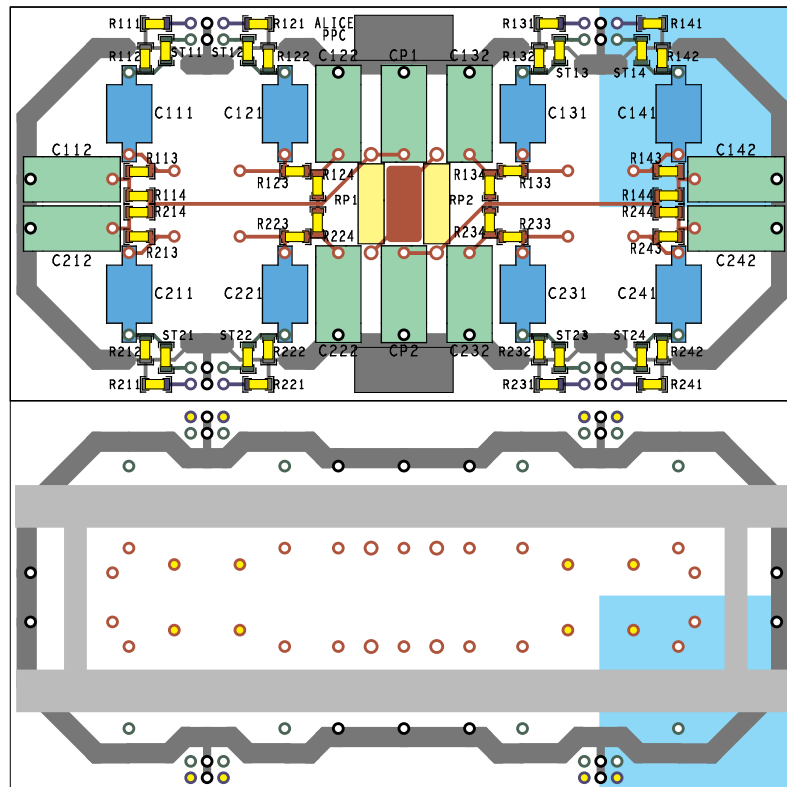


Figure 4: Detector PCB layout on the component side (top) and on the detector side (bottom) of one HV distribution unit serving eight detector cells. The light-grey bars in the bottom part indicate the plastic support bars for the detector cells.

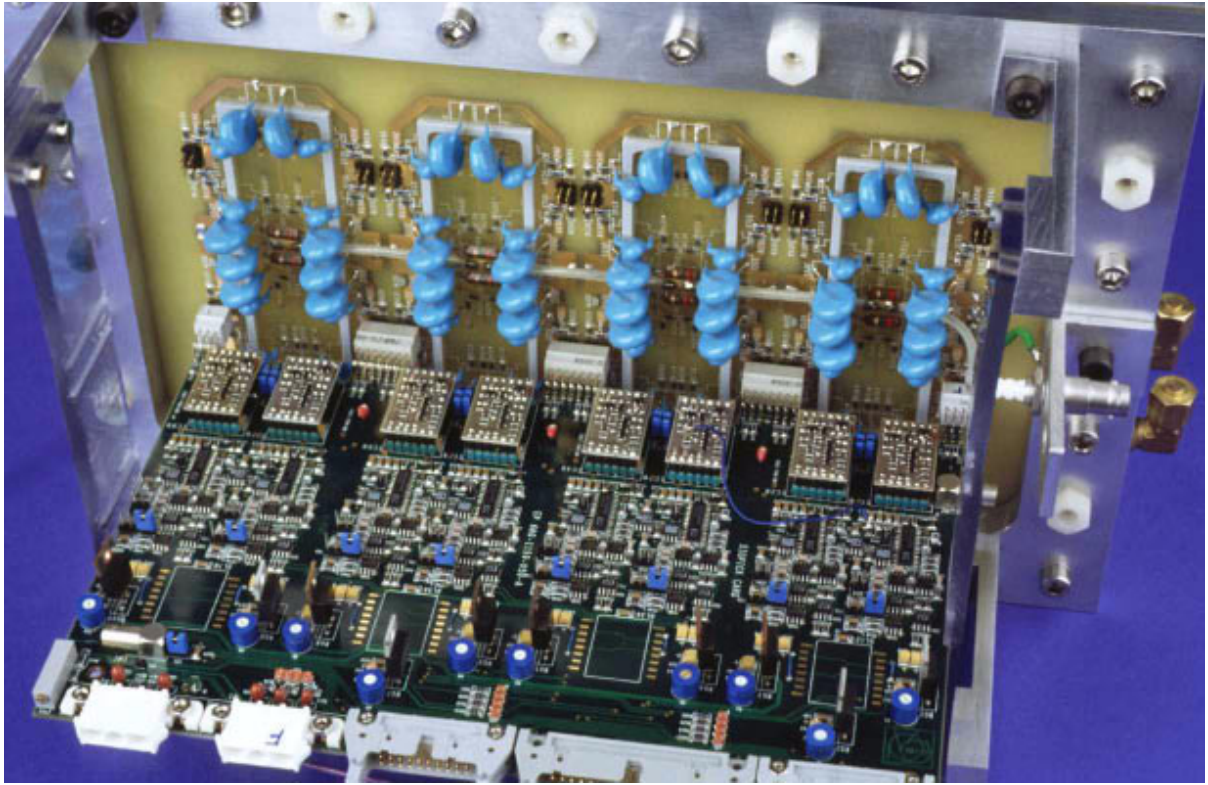


Figure 5: One eight-channel prototype readout card mounted on the prototype. The card carries amplifiers made with discrete components, discrimination logics and voltage regulation.

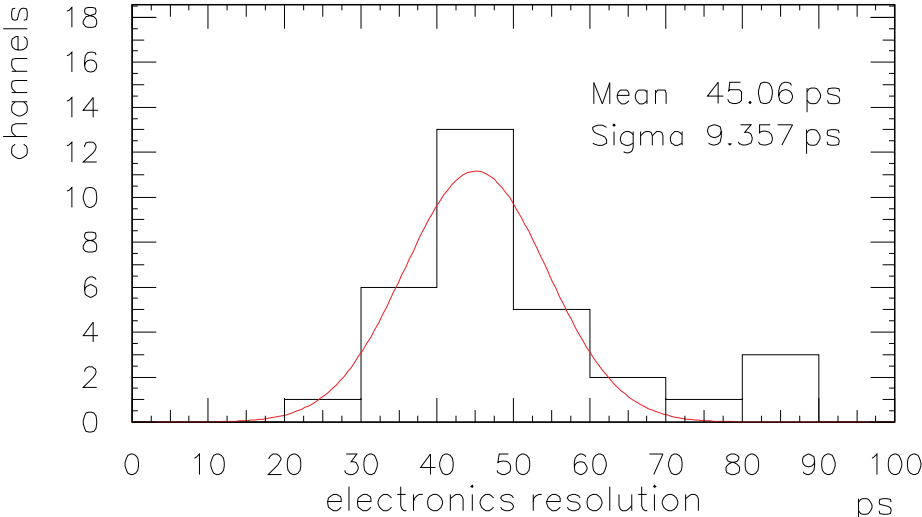


Figure 6: The distribution of time resolutions of all 32 electronics channels, measured by feeding all amplifiers with pulses of variable height triggered at random times. The parameters of a fitted Gaussian distribution are shown.

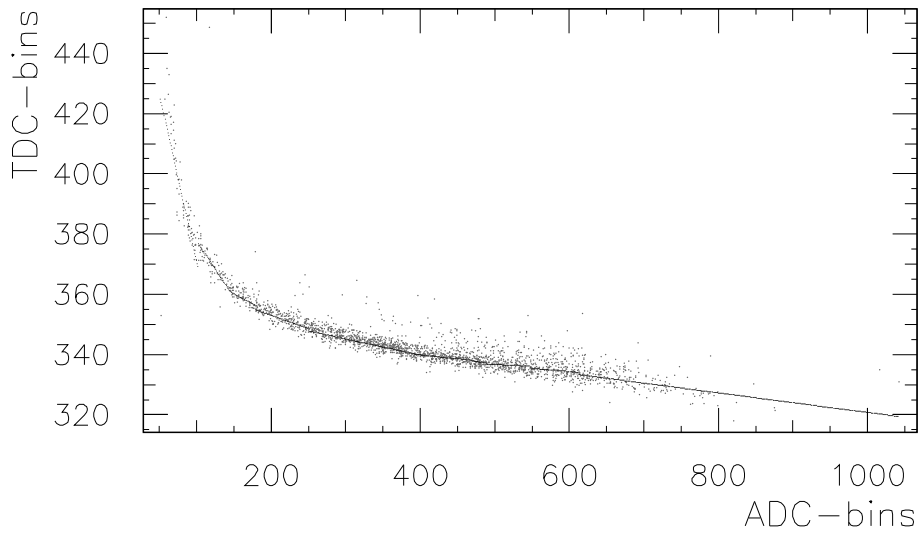


Figure 7: Time-amplitude correlation with correction curve for one of the channels in the array

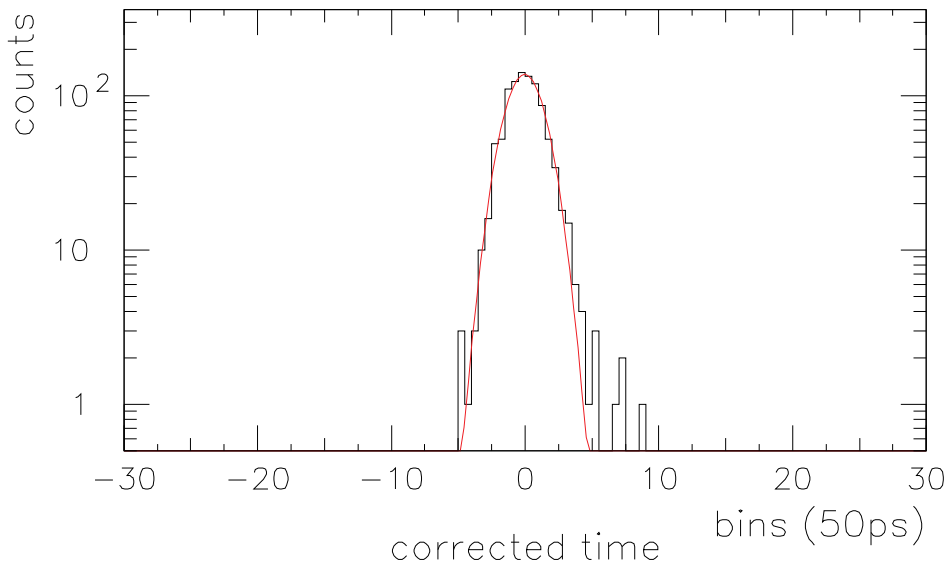


Figure 8: Distribution of the corrected time with fitted Gaussian distribution. 1.5% of the events are outside the fitted distribution.

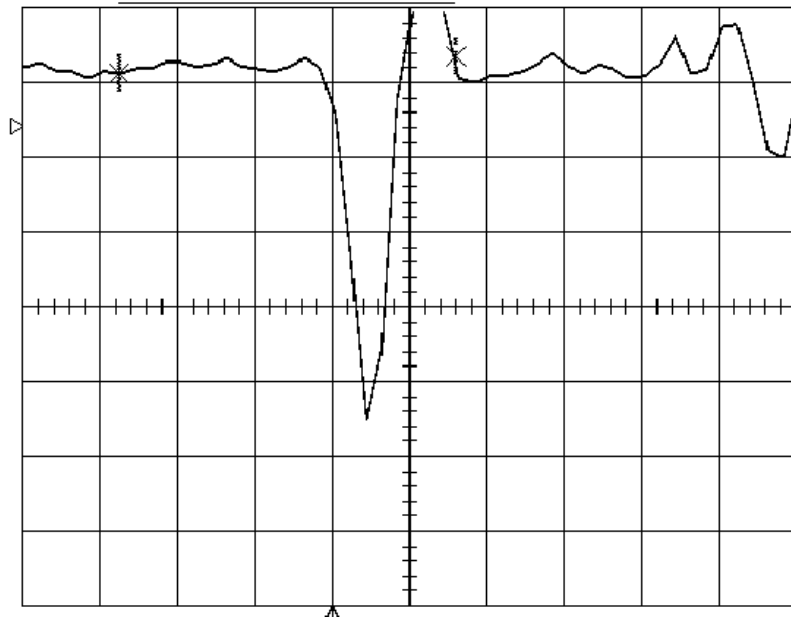


Figure 9: Typical proportional signal seen directly on $50\ \Omega$: $40\ \mu\text{A}/\text{div}$, $5\ \text{ns}/\text{div}$; $0.2\ \text{pC}/\text{square}$.

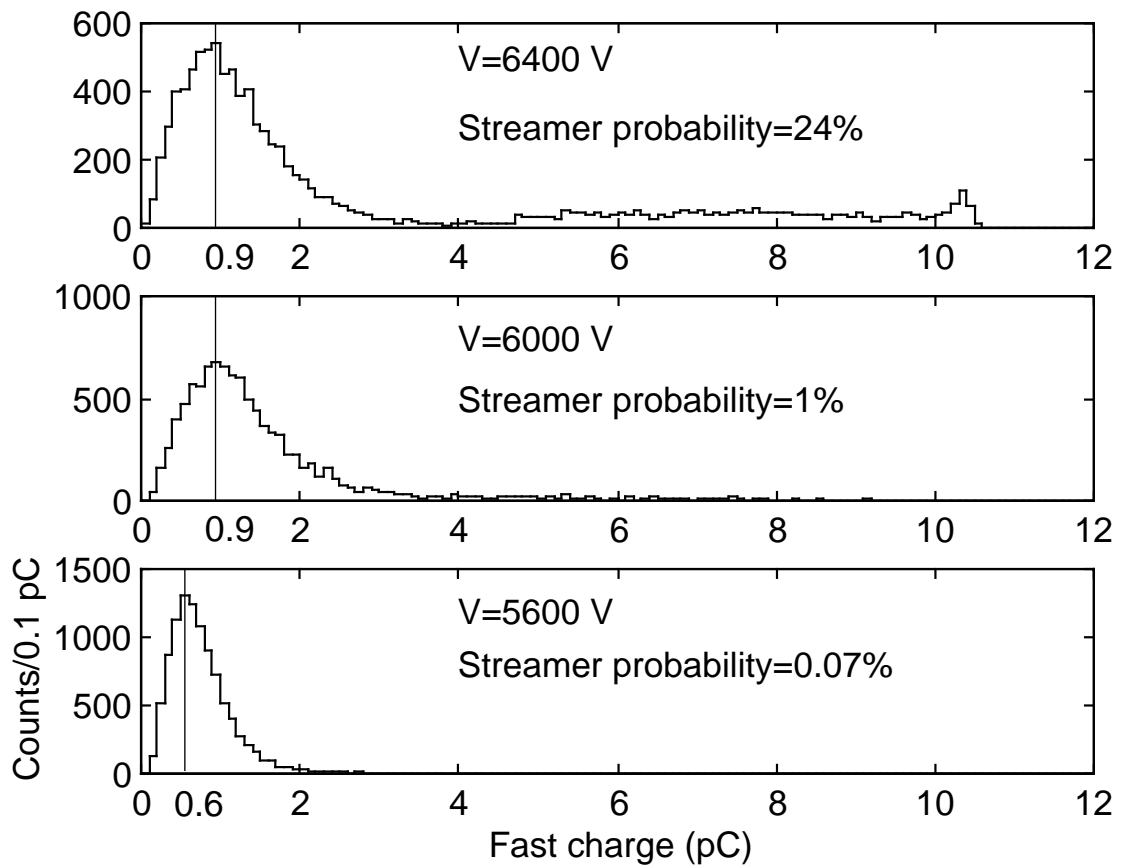


Figure 10: Pulse height spectra of $7\ \text{GeV}/c$ pions at different operating voltages.

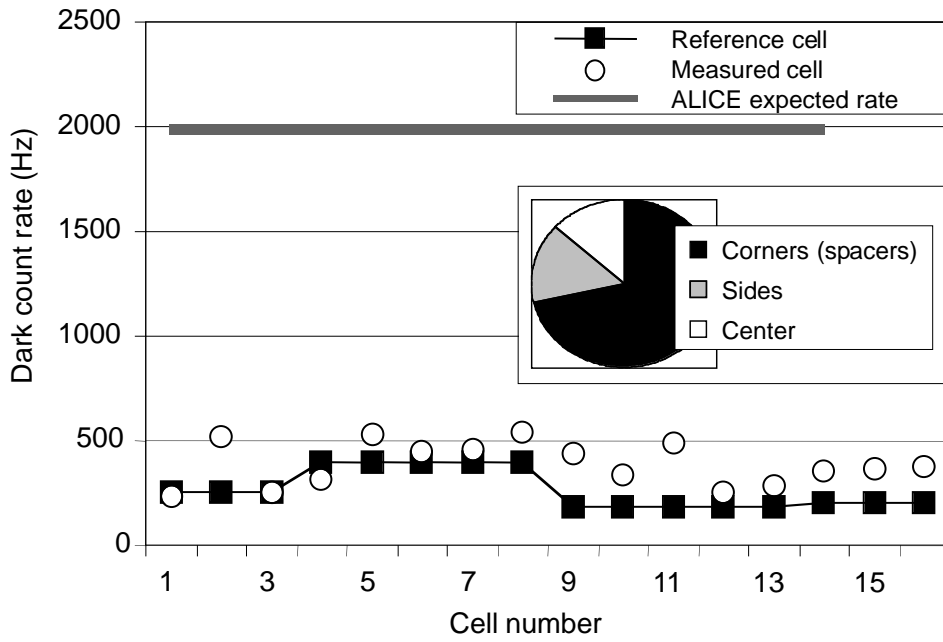


Figure 11: Dark count rate of glass-RPC cells. One identical reference cell has been measured together with each of the 16 cells. The pulses come mainly from the spacer region in the corners of the cells. The observed rates are one order of magnitude below the expected particle rate in the ALICE environment.

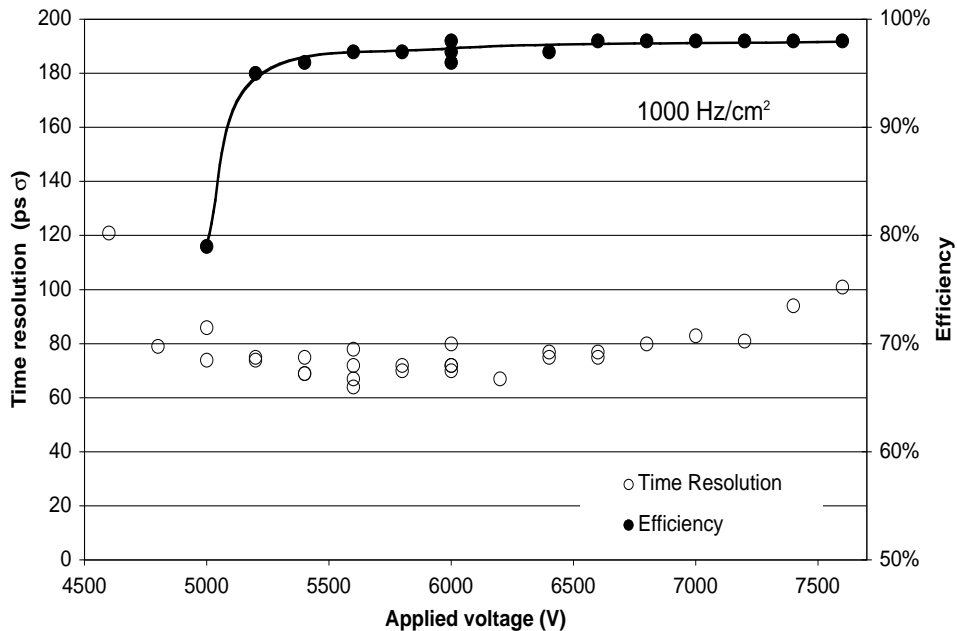


Figure 12: Detector time resolution and efficiency as a function of high voltage. The discriminator threshold was 20 fC, the particles rate 1000 Hz/cm².

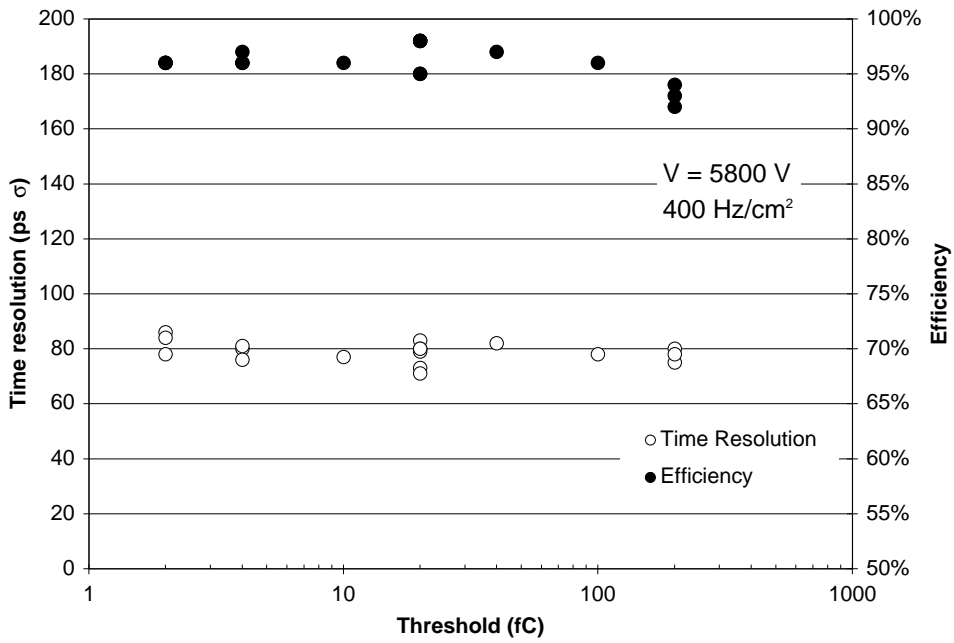


Figure 13: Detector efficiency and time resolution as a function of discriminator threshold. The operating voltage was 5800 V and the particle rate 400 Hz/cm². The spread of individual measurements under the same conditions is ~ 10 ps.

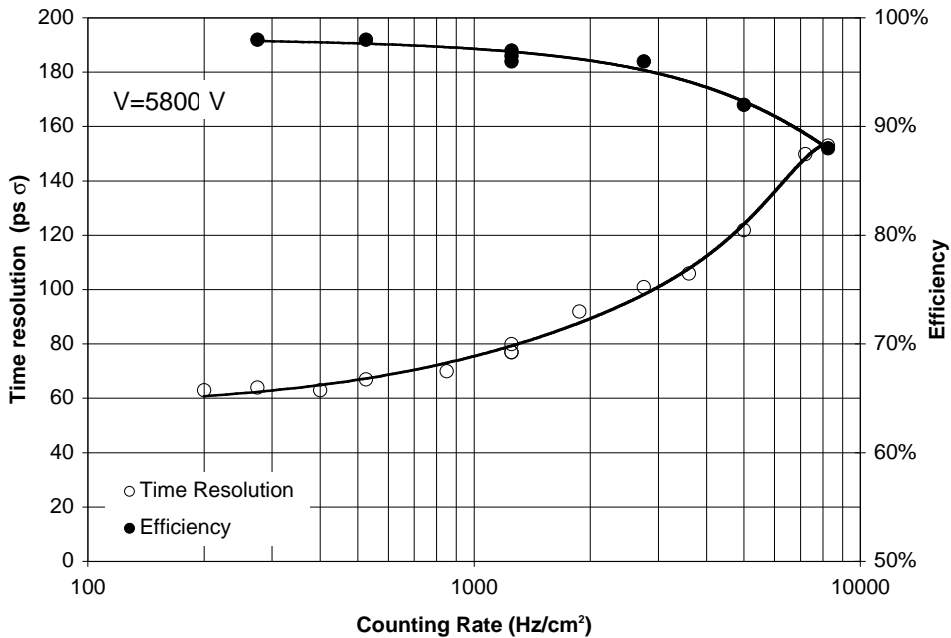


Figure 14: The time resolution and efficiency as a function of the beam particles rate. The operating voltage was 5800V and the discriminator threshold 20 fC.

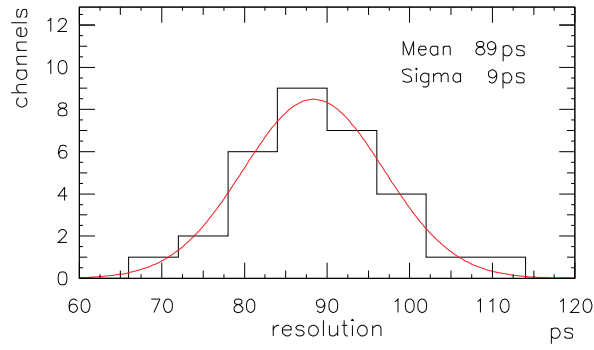


Figure 15: Distribution of measured time resolutions in the glass-RPC array with a fitted Gaussian distribution. The statistical parameters of the distribution are given.

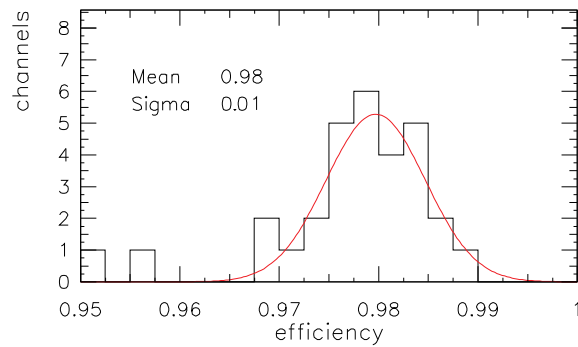


Figure 16: Efficiency distribution in the glass-RPC array with fitted Gaussian distribution. The statistical parameters of the full distribution are shown.

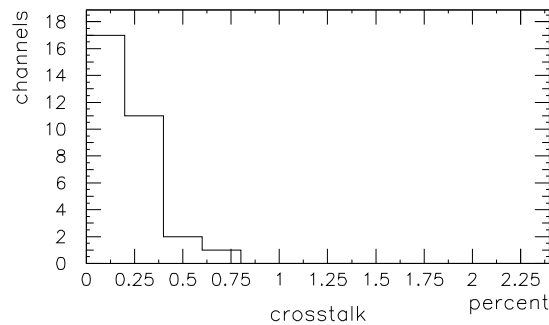


Figure 17: Distribution of crosstalk from 31 detector cells.

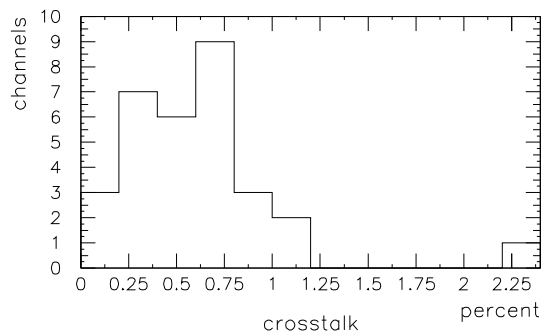


Figure 18: Distribution of crosstalk to neighbors from 31 channels.